Isotopes in Environmental and Health Studies, 2015
Vol. 51, No. 2, 231–254, http://dx.doi.org/10.1080/10256016.2015.1008468

Taylor & Francis
Taylor & Francis Group

Isotope hydrology and baseflow geochemistry in natural and human-altered watersheds in the Inland Pacific Northwest, USA

Ricardo Sánchez-Murillo[a,b*], Erin S Brooks[c], William J Elliot[d] and Jan Boll[a,c]

[a]*Waters of the West – Water Resources Program, University of Idaho, Moscow, ID, USA;* [b]*Chemistry Department, Universidad Nacional, Heredia, Costa Rica;* [c]*Department of Biological and Agricultural Engineering, University of Idaho, Moscow, ID, USA;* [d]*USDA Forest Service Rocky Mountain Research Station, Moscow, ID, USA*

(*Received 13 July 2014; accepted 29 November 2014*)

This study presents a stable isotope hydrology and geochemical analysis in the inland Pacific Northwest (PNW) of the USA. Isotope ratios were used to estimate mean transit times (MTTs) in natural and human-altered watersheds using the FLOWPC program. Isotope ratios in precipitation resulted in a regional meteoric water line of $\delta^2H = 7.42{\cdot}\delta^{18}O + 0.88$ ($n = 316$; $r^2 = 0.97$). Isotope compositions exhibited a strong temperature-dependent seasonality. Despite this seasonal variation, the stream $\delta^{18}O$ variation was small. A significant regression ($\tau = 0.11D^{-1.09}$; $r^2 = 0.83$) between baseflow MTTs and the damping ratio was found. Baseflow MTTs ranged from 0.4 to 0.6 years (human-altered), 0.7 to 1.7 years (mining-altered), and 0.7 to 3.2 years (forested). Greater MTTs were represented by more homogenous aqueous chemistry whereas smaller MTTs resulted in more dynamic compositions. The isotope and geochemical data presented provide a baseline for future hydrological modelling in the inland PNW.

Keywords: baseflow geochemistry; hydrogen-2; isotope hydrology; mean transit times; natural and human-altered watersheds; oxygen-18; watershed management

1. Introduction

In the Pacific Northwest (PNW) region of the USA, rapid population growth expected from ~ 15 million today to $\sim 85-100$ million by 2100 [1] has led to an increasing debate over competing water supplies and diverse interests (i.e. ecological, agricultural, socio-economical, cultural) [2–9]. The central pillar of this debate relies on the scientific recognition of the PNW as a particularly sensitive region to climate variability [3,4,7,10–14], which may result in significant hydrologic and stream temperature regime alterations. Overall, future climate scenarios for the PNW predict a warming of 0.1–0.6 °C per decade in the twenty-first century [15].

The inland PNW is bounded by the Cascades Mountains on the west and the Rocky Mountains on the east. This area comprises a variety of semi-arid and snow-dominated landscapes across Washington and Idaho that exhibit intrinsic hydrological feedbacks. For example, lower elevation areas that may experience more evapotranspiration in the future depend on the water supply from higher elevation snow-dominated watersheds, which, at the same time, may be potentially shifting from snow to rainfall domains coupled with earlier spring runoff events in

*Corresponding author. Email: sanc7767@vandals.uidaho.edu

a warmer climate [10]. Consequently, future hydro-climate scenarios in the inland PNW may affect: (a) the demand of groundwater supplies, electricity generation, clean drinking water, and recreation activities, which may converge in individual and inter-state water rights debates; (b) current water quality criteria under baseflow conditions; (c) disruption of ecological assemblages (e.g. high water temperatures, low dissolved oxygen concentrations) along summer flows which are critical to many ecosystems such as salmon rearing habitats. Hence, one imperative need that emerges from the aforementioned scenarios is to improve our understanding of the hydrological connectivity between the semi-arid and snow-dominated landscapes in the inland PNW.

To our knowledge, no comprehensive isotope hydrology assessments of precipitation and surface waters in the inland PNW of Washington and Idaho have been undertaken; rather isotopic research has been limited and site-specific [16–21]. Stable isotope and geochemical data are needed to create a baseline for future water resources assessments and modelling efforts in the inland PNW. The objectives of this study, therefore, were to use the stable isotopes of water to: (a) establish foundational regional and local meteoric water lines (LMWLs) in the inland PNW; (b) describe spatial and temporal isotopic variations in precipitation and surface waters; and (c) evaluate differences in mean transit times (MTTs) and transit time distribution (TTD) functions at variable catchment scales (10^0–10^2 km^2), land uses (i.e. agricultural–urban, mining, and forested), climatic gradients, and the main underlying geology (i.e. basalt, granitic, metamorphic, and sedimentary). MTT input–output relationships were constructed from δ^{18}O ratios in precipitation and surface waters over a sampling period of two years in most of the selected watersheds. The stable isotope data were complemented by a baseflow geochemical analysis conducted in five natural and human-altered watersheds to evaluate water quality conditions in these systems during the critical summer months.

1.1. *Stable isotope basics*

The use of stable isotopes of water, both deuterium (δ^2H) and oxygen-18 (δ^{18}O), has provided novel insights into the understanding of subsurface water movement, storage, and mixing processes [22]. The development of new instrumentation based on laser spectroscopy in recent years has improved the temporal resolution of isotopic data, reduced the analytical uncertainty and analysis timeframe [23–27], and provided new research avenues of the atmospheric water cycle (i.e. ^{17}O-excess) [28]. Particularly, these naturally occurring tracers have been recognized as a useful technique to study solute transport from column and plot studies [29], to watershed MTTs [30–35], and widely to elucidate atmospheric moisture sources and their implications in the hydrological cycle [36–42].

The global relationship between δ^2H and δ^{18}O in natural meteoric waters (i.e. continental precipitation that has not experienced evaporation), recognized by Craig [43] and later known as the Global Meteoric Water Line (GMWL: $\delta^2\mathrm{H} = 8{\cdot}\delta^{18}\mathrm{O} + 10$), serves as a foundational reference to determine regional or local deviations (i.e. local meteoric water line, LMWL) from equilibrium processes. Other factors such as the trajectory of air masses, latitude, altitude, precipitation amount, and distance to the coast may also affect the spatial and temporal variations of δ^2H and δ^{18}O in precipitation [36]. The GMWL slope of 8 is determined by the ratio between the equilibrium isotope fractionation effects of hydrogen (^{2}H/^{1}H) and oxygen (^{18}O/^{16}O), while the intercept 10 is controlled by the kinetic isotope fractionation occurring during non-equilibrium processes such as evaporation [25,43–45]. Water losses due to evaporation, the incorporation of recycled atmospheric moisture or mixing between isotopically distinct reservoirs leave a unique water fingerprint that can be used to understand rainfall-runoff processes [46], complex water flow paths [47], and groundwater to surface water connectivity [48–50]. In temperate regions,

isotopic variations in precipitation have been frequently correlated to mean surface air temperature at the sampling site [36,39,50,51]. In contrast, the deuterium excess or d-excess ($d = \delta^2H - 8{\cdot}\delta^{18}O$) [36] (i.e. a measure of the relative proportions of δ^2H and $\delta^{18}O$ in meteoric waters) is correlated with the physical conditions (i.e. relative humidity and sea surface temperature) of the oceanic source area [52]; therefore, the combination of δ^2H, $\delta^{18}O$, and d-excess can be used to understand hydrological processes from the origin of atmospheric moisture to evapotranspiration fluxes, runoff mechanisms, and groundwater recharge pathways.

1.2. *MTT theory*

The MTT or the time a water molecule or tracer spends travelling along subsurface flow pathways to the stream network is a fundamental hydraulic descriptor that provides useful information about water sources and mixing processes, potential flow pathways, and storage capabilities within a particular catchment control volume [31,53–56]. The conjugation of the MTT and the TTD characterizes the average discharge behaviour of a catchment [57–60], and consequently, describes how groundwater systems hold and release water, which is a key component of contaminant transport assessments and water resources management. While a unified criterion of catchment controls on MTT and the shape of TTD is unrealistic due the inherent complexity of water flow paths and geomorphologic heterogeneities across landscapes, several studies have found significant correlations between MTT and catchment characteristics such as flow path depth (e.g. mountainous catchment, Central Japan [61]), storage within the unsaturated zone (e.g. humid catchment, New Zeeland [53]), slope direction and exposure (e.g. Redondo Peak, New Mexico [62]), soil cover (e.g. Cairngorm mountains, Scotland [63]), and topography (e.g. mountainous catchments, Oregon [64]).

The MTT is usually estimated from the input–output dynamic of conservative tracers such as δ^2H, $\delta^{18}O$, and chloride [30,32,61,65–68], which involves fitting an average TTD (i.e. assumed to be time-invariant) using inverse modelling approaches with lumped convolution integral models [58,69–71]. The transport of the conservative tracer through a catchment can be described by the convolution integral (Equation 1):

$$\delta_{out}(t) = \int_0^\infty g(\tau)\delta_{in}(t-\tau)d\tau = g(t)*\delta_{in}(t), \tag{1}$$

where $\delta_{in}(t)$ and $\delta_{out}(t)$ are the tracer input and output compositions at any time t, respectively, τ is the turnover time, and $g(t)$ is the weighting function describing the shape of the TTD. The weighting function of the tracer is equal to the weighted function of the water infiltrated into the system if: (a) the tracer is conservative; (b) the tracer is injected and measured proportionally to the volumetric flow rate; or (c) there are no stagnant waters in the system [72]. In the case of steady flow, the MTT is defined by Equation 2:

$$\tau = \int_0^\infty tg(t)dt = \frac{V}{Q}, \tag{2}$$

where V (L^3) is the volume of mobile water in the system, Q ($L^3\ t^{-1}$) is the volumetric flow rate through the system, t is the time variable, and $g(t)$ is the weighting function. Several models have been proposed [69] (Table 1 and Figure 1) to describe the TTD function. The Piston Flow Model (PFM) is the simplest and less reliable distribution representation. This model assumes that water travels at equal velocities along all flow paths which is never true in a catchment (i.e. hydrodynamic dispersion and diffusion are negligible); this mechanism is represented by a single pulse. The Exponential Model (EM) assumes that the tracer transport occurs in a system where flow paths are distributed exponentially (i.e. equivalent to the response function of a well-mixed

Table 1. Weighting functions proposed by Maloszewski and Zuber [69].

Model	Weighting function g(t)[a]	Parameters	Variance
PFM	$\delta(t-\tau)$	τ	0
EM	$\tau^{-1}\exp\left(\frac{-t}{\tau}\right)$	τ	τ^2
EPM	$\frac{\eta}{\tau}\exp\left(-\frac{\eta t}{\tau}+\eta-1\right)$ for $t \geq \tau(1-\eta^{-1})$ 0 for $< \tau(1-\eta^{-1})$	$\tau,\ \eta$	$\left(\frac{\tau}{\eta}\right)^2$
DM	$\left(\frac{4\pi D_p t}{\tau}\right)^{-(1/2)} t^{-1}\exp\left[-\left(1-\frac{t}{\tau}\right)^2\left(\frac{\tau}{4\pi D_p t}\right)\right]$	$\tau, D_p = \frac{D}{vx}$	$\tau^2\left(2\frac{D}{vx}\right)$

[a] τ is the MTT, D_p is the apparent dispersion parameter ($D_p = D/vx$, the reciprocal of the Péclet number, which describes the ratio of the dispersion to advection), η is the ratio of the total volume to the volume with the exponential distribution of transit times, and $(t-\tau)$ is the Dirac delta function.

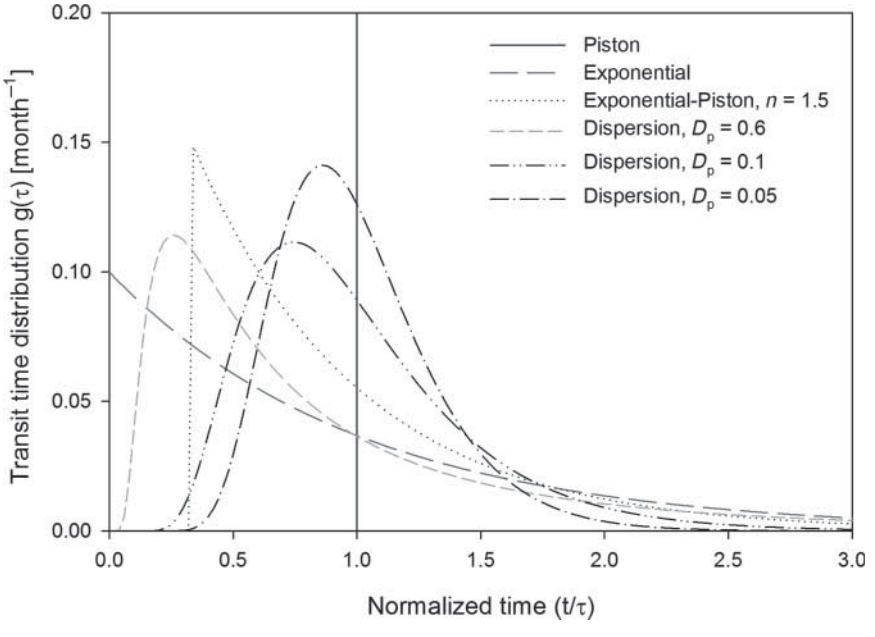

Figure 1. Examples of common MTT distribution functions (TTD) used in FLOWPC simulations.

reservoir). The Dispersion Model (DM) can take several forms depending on the dispersion parameter D_p. The Exponential Piston Model (EPM) describes a system that is exponentially distributed but is delayed in time.

2. Study area

The study watersheds are located within the inland PNW in three areas of particular hydrological interest: Palouse region, Silver Valley, and Priest River (Figure 2). The study sites include a variety of climatic gradients, geologic features, and natural and human-altered watersheds. A summary of hydrogeological characteristics in each study area is presented herein. Additional information in five selected watersheds is presented in the Supplemental online materials (Tables S1 and S2).

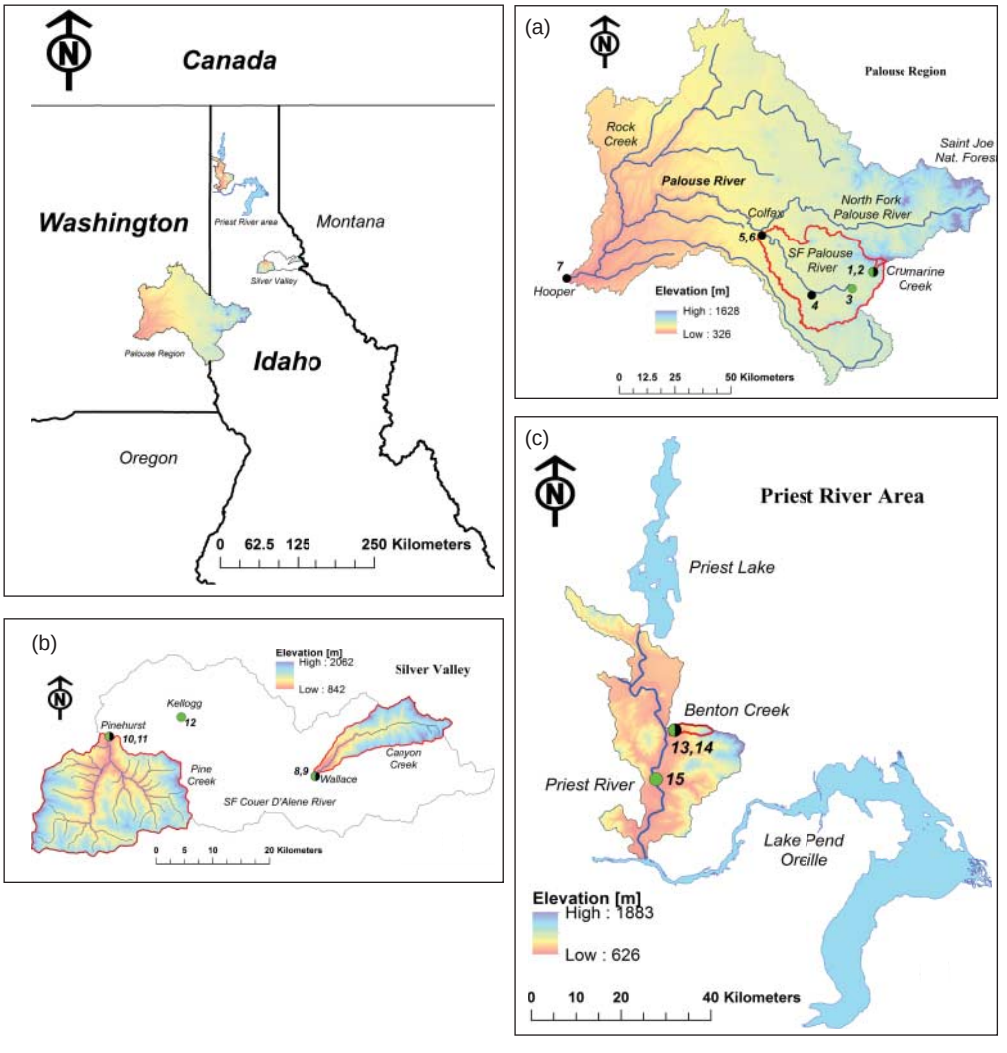

Figure 2. Study watersheds showing elevation (*m*), main locations and streams, and surface water (black circles) and precipitation (green circles) sampling stations. Semi-filled circles denote stations where both stream and precipitation samples were collected. The inset shows an overview of study area within the inland PNW, USA. (a) PRB includes sampling points 1–2 (Crumarine Creek), 3 (Moscow, ID), 4 (South Fork Palouse River, Pullman, WA), 5–6 (North and South tributaries of the Palouse River), and 7 (Hooper, WA). (b) Pine Creek and Canyon Creek catchments comprise locations 8–9 (Wallace, ID), 10–11 (Pinehurst, ID), and 12 (Kellogg, ID). (c) Lower Priest River watershed includes sampling points 12–14 (Benton Creek), and 5 (Priest River, ID).

2.1. *Palouse region*

The Palouse region is located on the western slopes of the Saint Joe and Clearwater National Forests (Figure 2(a)) covering roughly 9000 km^2 of which 60 % corresponds to croplands (i.e. wheat and legumes) [73,74] throughout Washington's Whitman County and Idaho's Latah County. The Palouse River Basin (PRB) is part of the eastern Columbia Plateau and its geology is divided in three main features: (a) pre-tertiary crystalline basement rock: (b) Miocene basalt flows and associated sedimentary interbeds of the Latah Formation; and (c) thick Quaternary loess deposits [75]. Mean annual precipitation ranges from 462 mm in the east to 1188 mm in

the west [74]. In recent years, drinking water availability has been a matter of concern in the area due to the steady decline in groundwater levels on the order of 30 cm per year [76].

Stable isotope hydrology was studied in three nested watersheds within the Palouse Basin: Palouse River (Hooper, WA), North and South Forks of the Palouse River (Colfax, WA) (Figure 2(a)). These watersheds were selected to determine the spatial and temporal (i.e. monthly) isotopic variability in surface waters at meso ($\sim 10^2$ km^2) and large scales ($\sim 10^3$ km^2). Isotopic variations at a finer time resolution (i.e. weekly and storm basis) and baseflow geochemistry were studied in two watersheds: South Fork of the Palouse River (Pullman, WA) and Crumarine Creek (Moscow, ID) (Figure 2(a)).

The South Fork of the Palouse River (Pullman, WA) comprises a drainage area of 342 km^2 over agricultural and urban areas (Moscow, Idaho and Pullman, Washington). Basalts of the Columbia River group covered by deposits of clayey silt loess compose the main bedrock geology feature (64.7 %). Mean watershed slope is 12 %. Total stream length corresponds to 586 km. Mean annual temperature is 8.22 °C. Mean annual precipitation and discharge are 670 and 97 mm/yr, respectively. Crumarine Creek is a small forested (i.e. coniferous) watershed with a drainage area of 6.35 km^2. Mean landscape slope is 28.4 % with a total stream length of 8 km. Mean annual temperature is 7.27 °C. Mean annual precipitation and discharge are 790 and 230 mm/yr, respectively. The watershed is entirely composed of granitic rock producing stream beds of weathered granite.

2.2. *Silver Valley area*

The Silver Valley also known as the Coeur d'Alene (CDA) mining district is a narrow valley ($\sim$64 km long) in the panhandle of northern Idaho (Figure 2(b)) affected since the 1880s by mineral exploration and ore processing (i.e. 90 historical mines of silver, zinc, cooper, antimony, gold, and lead). The Silver Valley contains the largest underground mine in the USA (Bunker Hill Mine, with over 150 miles of workings), the deepest mine (Star-Morning, which is over 2.6 km deep), and the richest silver mine (Sunshine, which has produced over 10,000 metric tons of silver) [77]. Until late 1968, when tailing ponds were established, most of the heavy metal-enriched wastes ($\sim$2200 metric ton/day) were transported via the South Fork of the CDA River to Lake CDA [78].

Stable isotope hydrology and baseflow geochemistry were studied in two mining-altered watersheds (i.e. Pine Creek and Canyon Creek) located within the Silver Valley (Figure 2(b)). Pine Creek comprises 190 km^2 of snow-dominated forested landscape with a mean watershed slope of 46.5 %. Mean annual precipitation and discharge are 1225 and 703 mm/yr, respectively. Mean annual temperature is 5.46 °C. Main underlying geology units are metamorphic (63.1 %) and sedimentary (36.9 %). Pine Creek flows into the South Fork of the CDA River near the city of Pinehurst, Idaho. The Canyon Creek drainage hosted over 30 lead and silver mines and 8 mills by 1978 (Silver Valley Natural Resource Trustees, 2000). Historical lead concentrations in floodplain sediments range from 3540 to 136,000 mg/kg [79]. Canyon Creek drainage area is 60 km^2 with an average catchment slope of 46.3 %. Mean annual precipitation and discharge are 1313 and 754 mm/yr, respectively. Mean annual temperature is 3.81 °C. Canyon Creek geology is mainly metamorphic (66.1 %), sedimentary (17.8 %), and alluvial deposits (12.9 %). Canyon Creek flows into the South Fork of the CDA River above the city of Wallace, Idaho.

2.3. *Priest River area*

The Priest River functions as a hydrological connection between Priest Lake and the Pend Oreille River (Figure 2(c)). Priest River's regional geology is mainly composed of an igneous and

metamorphic culmination complex [80]. The Priest River Experimental Forest (PREF) is located on the western slopes of the Selkirk Mountains in northern Idaho with 90 % of the land area in pristine coniferous forest. Elevation ranges from 626 to 1883 m. Three main drainages within the PREF are tributaries of the Priest River: Benton Creek, Canyon Creek, and Fox Creek. Stable isotope hydrology and baseflow geochemistry was studied in Benton Creek with drainage area of 7.24 km^2 (Figure 2(c)). Mean watershed slope is 34.7 %. Mean annual temperature is 5.67 °C. Mean annual precipitation and discharge are 847 and 240 mm/yr, respectively. Main bedrock geology is composed of granite (64.6 %) and metamorphic (32.2 %) features. Additionally, stable isotope samples were collected in Priest River near the city of Priest River, Idaho.

3. Methods and materials

3.1. *Stable isotope analyses*

Precipitation was collected (1–2 weeks composite samples, see Supplementary Table S5) through passive collectors composed of a Buchner funnel (11.0 cm diameter; Fischer Scientific, USA) coupled with a fabric filter mesh (3 mm diameter) to prevent sample contamination (e.g. dust, pollen, insects, debris). The funnel was connected to a 4-L high density polyethylene (HDPE) container using silicone tubing (1 cm diameter). A 2-cm thick mineral oil (Aspen Veterinary Resources Ltd., USA) layer was added to prevent fractionation according to standard sampling protocols [22]. Mineral oil was separated using a 500 mL glass separatory funnel (Fischer Scientific). Samples were stored upside down at 5 °C in 30-mL glass E-C borosilicate bottles with tetrafluoroethylene (TFE)-lined caps (Wheaton Science Products, USA). Bottles were filled with no head space and covered with parafilm (Thermo Scientific, USA) to avoid exchange with atmospheric moisture. Snow samples were collected using a snow sampler Model 3600 (4.13 cm, diameter) (Rickly Hydrological Company, USA). Snow cores were melted in sealed plastic bags. Samples were immediately transferred and stored upside down at 5 °C in 30-mL glass E-C borosilicate bottles with TFE-lined caps (Wheaton Science Products, USA).

Surface water samples were collected using an automated sampler ISCO 3700 (Teledyne ISCO, USA) on a weekly basis at fixed times (15:00 Pacific Standard Time) in each monitoring station. Storm sampling was conducted using a pressure transducer PT12 (INW, USA) connected to the automated sampler through a data logger CR10X (Campbell Scientific, USA). A 2-cm thick mineral oil (Aspen Veterinary Resources Ltd.) layer was added to 1-L HDPE bottles to prevent evaporation during storage [22]. Mineral oil was separated using a 250-mL glass separatory funnel (Fischer Scientific). Manual samples were collected in 30-mL glass E-C borosilicate bottles with TFE-lined caps (Wheaton Science Products). Bottles were filled with no head space and covered with parafilm (Thermo Scientific) to prevent exchange with external moisture sources. All samples were stored upside down at 5 °C until analysis. Supplementary online materials (Table S3 and S4) present a summary of surface water and precipitation sampling locations in the inland PNW, including site identification, geographic coordinates, station elevation, period of record, number of samples, and sampling frequency. Daily discharge records were obtained from the United States Geological Survey National Water Information System (http://waterdata.usgs.gov/nwis).

Stable isotope analyses were conducted at the Idaho Stable Isotope Laboratory, University of Idaho (Idaho, USA) using a Cavity Ring Down Spectroscopy water isotope analyzer L1120-i (Picarro, USA) following the methods described by Lis et al. [24]. Laboratory standards, previously calibrated to the VSMOW2-SLAP2 reference waters, were EAG ($\delta^2H = -255.0$ ‰, $\delta^{18}O = -30.8$ ‰), CAS ($\delta^2H = -64.2$ ‰, $\delta^{18}O = -8.3$ ‰), and DDI ($\delta^2H = -15.4$ ‰,

$\delta^{18}O = -125.5$ ‰). EAG and CAS were used to normalize the results to the VSMOW2-SLAP2 scale while DDI was a quality control standard. The laboratory precision on average was ± 0.5 ‰ (1σ) for $\delta^{2}H$ and ± 0.1 ‰ (1σ) for $\delta^{18}O$. The estimated *d*-excess analytical uncertainty was ± 0.6 ‰ (1σ).

Periodic regression analysis [81] was used to fit a seasonal sine-wave model to $\delta^{18}O$ fluctuations as:

$$\delta^{18}O_p = \delta^{18}\overline{O} + A[\cos(ct - \theta)], \tag{3}$$

where $\delta^{18}O_p$ is the predicted $\delta^{18}O$ in ‰, $\delta^{18}\overline{O}$ is the annual mean $\delta^{18}O$ value in ‰, A is $\delta^{18}O$ annual amplitude in ‰, c is the radial frequency of annual fluctuations or 0.017214 rad d^{-1}, t is time in days after the beginning of the sampling, and θ is the phase lag or time of annual peak $\delta^{18}O$ in radians. The damping ratio (D) of the precipitation isotopic signal in the observed stream isotopic response was calculated as the ratio of the standard deviation of stream water isotopic composition (i.e. all data points) (SD_s) to the standard deviation of precipitation isotopic composition (SD_p) [82]:

$$D = \frac{SD_s}{SD_p}. \tag{4}$$

Additionally, a preliminary estimation of MTTs was conducted using the exponential well-mixed model [69]:

$$\tau = c^{-1}[(D)^{-2} - 1]^{0.5}, \tag{5}$$

where τ is the MTT in days, c is the radial frequency of annual fluctuations or 0.017214 rad d^{-1}, $\delta^{18}O_s$ and $\delta^{18}O_p$ correspond to the $\delta^{18}O$ amplitudes in the stream and precipitation, respectively.

3.2. *Baseflow MTT simulations*

Baseflow MTTs were estimated using the lumped-parameter computer program FLOWPC 3.2 (http://www-naweb.iaea.org/napc/ih/IHS_resources_sampling.html) [70] in five selected watersheds (i.e. SF Palouse River, Crumarine Creek, Pine Creek, Canyon Creek, and Benton Creek). Stream $\delta^{18}O$ values during runoff events were excluded, thus, the convolution age estimates were limited by the sample size of baseflow observations. FLOWPC has been widely applied to estimate MTT in several hydrologic applications [65,83–86]. Model parameters (τ,η, D/vx) for the different models (EM, EPM, DM) were obtained by trial and error in order to fit measured output isotope ratios. In FLOWPC, the goodness of the fit is determined as:

$$\sigma = \frac{\sqrt{\sum_{i=0}^{n}(C_m - C_p)^2}}{n}, \tag{6}$$

where C_m and C_p are the measured and predicted tracer compositions, n is the number of observations. In order to complement the evaluation of the simulations in FLOWPC, other authors [65,87] have suggested the incorporation of the following goodness of fit criteria (Table 2): index of agreement d [88], root mean square error RMSE, and the mean absolute error MAE. The index of agreement d intends to overcome the insensitivity of the coefficient of determination r^2 to differences in the observed and predicted means and variances [89]. The index of agreement d ranges from 0 (i.e. no correlation) to 1 (i.e. perfect fit). The MAE and RMSE are the errors that provide the absolute mean deviation from the measurements.

Table 2. Description of goodness of fit metrics used to evaluate FLOWPC simulations.

Metric	Function[a]	Reference
Root mean square error, RMSE	$\sqrt{\frac{1}{n}\cdot\sum_{i=1}^{n}(C_p - C_m)^2}$	Stumpp et al. [87]
Index of agreement, *d*	$1 - \frac{\sum_{i=1}^{n}(C_m - C_p)^2}{\sum_{i=1}^{n}(\lvert C_p - \bar{C}\rvert + \lvert C_m - \bar{C}\rvert)}$	Willmot [88]
Mean absolute error, MAE	$\frac{1}{n}\sum_{i=1}^{n}\lvert C_p - C_m\rvert$	Viville et al. [65]

[a] C_m, C_p, and $\bar{C}$ are the measured, predicted, and mean measured tracer compositions; n is the number of observations.

3.3. *Aqueous geochemistry*

A baseflow geochemical characterization was conducted during the 2013 summer (i.e. from 29 May to 17 September 2013) in five watersheds (i.e. Crumarine Creek, South Fork Palouse River, Canyon Creek, Pine Creek, and Benton Creek, Figure 2). Six manual samples were collected every three weeks in 125-mL HDPE bottles. Samples were filtered after arrival to the laboratory facilities. Extended alkalinity (i.e. total alkalinity, HCO_3^-, CO_3^{2-}, OH^-), pH, major anions (i.e. F^-, Cl^-, Br^-, NO_2^-, NO_3^-, PO_4^{3-}, and SO_4^{2-}), and dissolved metals (i.e. Ba, Ca, Cd, Co, Cr, Cu, Fe, K, Mg, Mn, Mo, Na, Ni, V, Zn) were analysed at the Analytical Sciences Laboratory, University of Idaho, USA. Additionally, dissolved Pb was analysed in two mining-altered watersheds (i.e. Pine Creek and Canyon Creek, Silver Valley, Figure 2(b)). Extended alkalinity samples were collected with no head space and immediately covered with Parafilm (Thermo Scientific, USA) to prevent atmospheric CO_2 exchange. Extended alkalinity was conducted by a titrimetric method [90]. The reporting limit averages 3 mg/L $CaCO_3$. Determination of inorganic anions was conducted by ion chromatography [91] using a Dionex DX-100 Ion Chromatograph. Reporting limits average 0.15 mg/L (F^-), 0.2 mg/L (Cl^-), 0.05 mg/L (NO_2–N), 0.1 mg/L (Br^-), 0.05 mg/L (NO_3–N), 0.1 mg/L (PO_4–P), and 0.2 mg/L (SO_4^{2-}). Dissolved metal samples were acidified *in situ* (i.e. pH $\sim$ 2) to avoid precipitates. Samples were analysed using Inductively Coupled Plasma Optical Emission Spectroscopy [92]. Dissolved Pb was analysed by Inductively Coupled Plasma Mass Spectrometry [93] (reporting limit 0.0025 µg/mL).

4. Results and discussion

4.1. *δ^2H and $\delta^{18}O$ in precipitation*

The δ^2H and $\delta^{18}O$ values of 316 precipitation samples collected in the Palouse region ($n = 203$), Silver Valley ($n = 87$), and Priest River area ($n = 26$) between September 2011 and January 2014 are presented in Figure 3. The precipitation isotope data are presented in the Supplemental online materials (Table S5). The δ^2H and $\delta^{18}O$ values of precipitation in the Palouse region ranged from -207.1 ‰ to -32.6 ‰ and from -27.7 ‰ to -4.5 ‰, respectively. A least squares regression of the precipitation isotope data resulted in a highly significant Palouse region meteoric water line (PMWL): $\delta^2H = 7.45 \cdot \delta^{18}O + 1.78$ ($r^2 = 0.97$, Figure 3). The simulated mean annual $\delta^{18}O$ composition of precipitation in the Palouse region was -14.7 ‰, with extremes ranging from -17.2 ‰ to -9.8 ‰. The δ^2H and $\delta^{18}O$ values in the Silver Valley ranged from -170.0 ‰ to -56.6 ‰ and from -22.7 ‰ to -6.7 ‰, respectively. A least

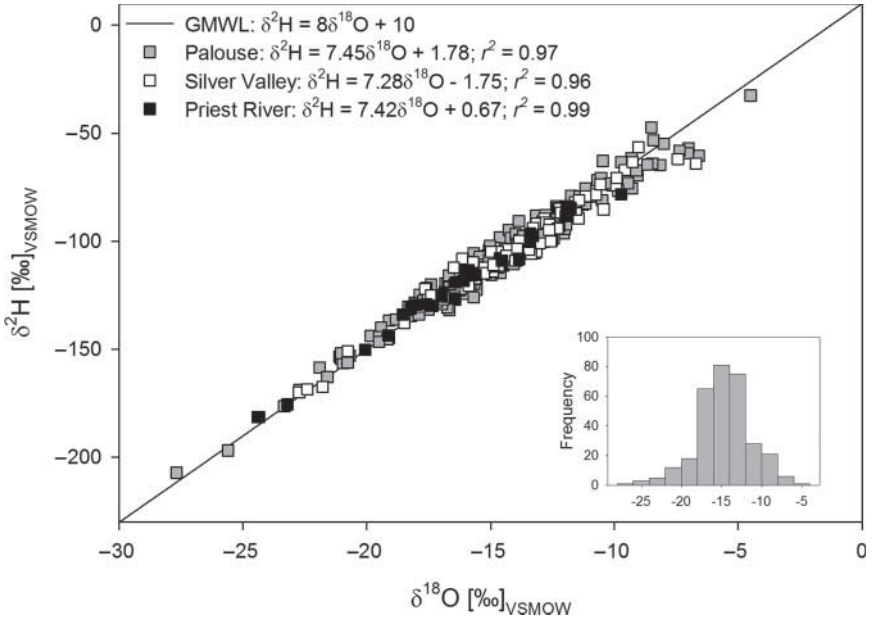

Figure 3. Isotopic composition of precipitation in the inland PNW, USA. Grey squares represent the PMWL ($n = 203$). Open squares correspond to the SVMWL ($n = 87$). Black squares denote the Priest River meteoric water line ($n = 26$). Local meteoric water lines are compared to the GMWL. Inset shows a distribution of $\delta^{18}O$ values among all the sampling sites.

squares regression of the precipitation isotope data resulted in a significant Silver Valley meteoric water line (SVMWL): $\delta^2H = 7.28 \cdot \delta^{18}O - 1.75$ ($r^2 = 0.96$, Figure 3). The simulated mean annual $\delta^{18}O$ composition of precipitation in the Silver Valley was -14.5 ‰, with $\delta^{18}O$ values ranging from -17.0 ‰ to -10.5 ‰. The δ^2H and $\delta^{18}O$ values in the Priest River area ranged from -181.3 ‰ to -78.2 ‰ and from -24.4 ‰ to -9.7 ‰, respectively. A least squares regression of the precipitation isotope data resulted in a significant Priest River area meteoric water line: $\delta^2H = 7.42 \cdot \delta^{18}O + 0.67$ ($r^2 = 0.99$, Figure 3). The simulated mean annual $\delta^{18}O$ composition of precipitation in the Priest River area was -16.2 ‰, with $\delta^{18}O$ values ranging from -18.5 ‰ to -11.5 ‰.

A Kruskall–Wallis non-parametric test revealed that there was no significant difference ($p = 0.086$) in the hydrogen and oxygen isotope data collected in the three study areas; therefore, an inland PNW meteoric water line based on all the precipitation samples can be described as: $\delta^2H = 7.42 \cdot \delta^{18}O + 0.88$ ($n = 316$; $r^2 = 0.97$). Long-term isotopic records (> 2 years) in precipitation within the inland PNW are scarce. Indeed, no stations are reported in the Global Network of Isotopes in Precipitation [94] data base of the International Atomic Energy Agency and the World Meteorological Organization. Previous site-specific studies in the inland PNW have reported few meteoric water lines that also presented lower slope and intercept values: $\delta^2H = 7.1 \cdot \delta^{18}O - 5$ (Palouse region, [19]) and $\delta^2H = 6.9 \cdot \delta^{18}O - 18.5$ (Palouse region, [16]. A 10-year LMWL was reported by Peng et al. [95] for Calgary, Canada (i.e. close to the Canada–US border above northern Idaho): $\delta^2H = 7.68 \cdot \delta^{18}O - 0.21$ ($n = 942$).

Low slope and intercept values are usually attributed to convective recycling processes [50]; especially in semi-arid regions where soil and surface water evaporation losses (i.e. moisture enriched in ^2H and ^{18}O) can mix with air masses resulting in lower slope values. Overall, δ^2H and $\delta^{18}O$ values in the inland PNW showed a temperature-dependent seasonality (Figure 4(a)). Enriched or more positive δ-values occurred during late spring and summer rains

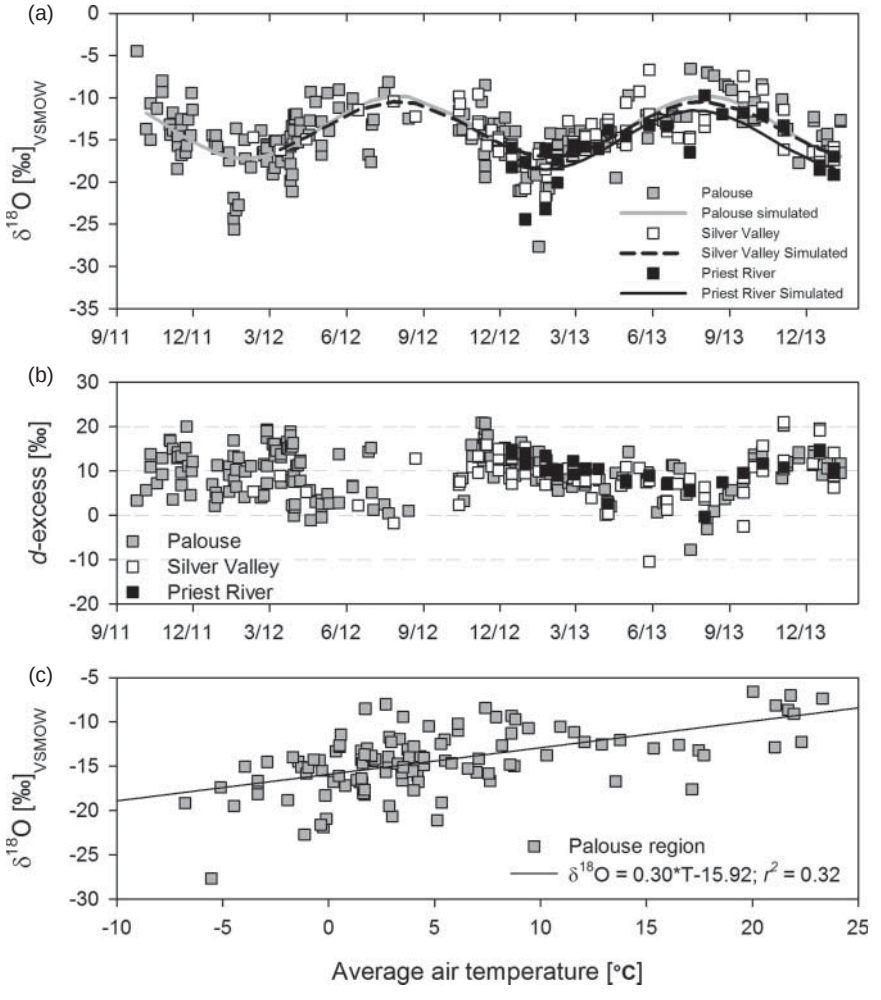

Figure 4. (a) Time series of $\delta^{18}O$ (‰) in precipitation for the Palouse region (grey squares), Silver Valley (open squares), and Priest River (black squares). Isotope values show a clear seasonality effect where depleted ratios occurred during winter and enriched ratios throughout the summer and early fall. Sine-wave $\delta^{18}O$ simulations are shown (grey line, Palouse region; black dash line, Silver Valley; black line, Priest River). (b) *d*-excess time series for Palouse region (grey squares), Silver Valley (open squares), and Priest River (black squares). The *d*-excess values were lowest in the summer and highest in the winter. (c) Relationship of average air temperature (°C) and $\delta^{18}O$ values in the Palouse region ($n = 203$).

(May–October) whereas lower or more negative δ-values were observed throughout the winter (November–April).

4.2. *Deuterium excess and temperature correlation*

The *d*-excess values of precipitation in the Palouse region, Silver Valley, and Priest River areas ranged from -7.8 ‰ to $+20.9$ ‰ (mean $= +9.8$ ‰), -10.5 ‰ to $+21.0$ ‰ (mean $= +8.7$ ‰), -0.4 ‰ to $+14.8$ ‰ (mean $= +10.0$ ‰) (Figure 4(b)), respectively, compared to the global mean *d*-excess $+10.0$ ‰. Positive deviations ($+10$ ‰ to $+30$ ‰) in *d*-excess values indicate enhanced moisture recycling whereas negative deviations (-10 ‰ to $+10$ ‰) correspond to an indication of mixing of evaporation losses [52]. Overall, *d-excess* values in the

Priest River area were less variable and reflect less influence of recycling moisture or secondary evaporation process than observed in the Palouse region and Silver Valley areas.

The lowest *d*-excess values were observed during the summer months and early fall whereas greater values were observed in the winter seasons (Figure 4(b)). Low *d*-excess values for precipitation in the inland PNW, particularly during the summer, revealed the incorporation of local recycled water vapour into the air mass and potential secondary evaporation of rainfall during small rain events (< 5 mm). In semi-arid regions, summer rainfalls from thunderstorms that obtain moisture mainly from local evapotranspiration are known to produce more negative *d*-excess values [50,95]. Basically, water drops below the cloud base may become isotopically more enriched in the heavy isotopes ^{2}H and ^{18}O by kinetic isotope effects during evaporation as they fall towards the ground surface [96–98]. The greater *d*-excess values observed ($+14.9$ ‰ to $+21$ ‰) during the winter are correlated with non-equilibrium conditions during the formation of snow [99] (Figure 4(b)).

The δ^{18}O values of precipitation in the Palouse region (2011–2014) and the average ground air temperature (T) during the sampling period are presented in Figure 4(c). The significant relationship ($p < .001$) between δ^{18}O values and average air temperature was $\delta^{18}\mathrm{O} = 0.30 \cdot T - 15.9$ ‰ ($r^2 = 0.32$) (Figure 4(c)). Lower air temperatures resulted in lower δ^{18}O values whereas greater temperatures are correlated with enriched ^{18}O, supporting the seasonal behaviour presented in Figure 4(a). This correlation ($\delta^{18}\mathrm{O} = 0.69 \cdot \mathrm{T} - 13.9$ ‰) was first observed by Dansgaard [36]. In the Calgary area, close to the northern Idaho US–Canada border ($\delta^{18}\mathrm{O} = 0.46 \cdot \mathrm{T} - 19.35$ ‰) Peng et al. [95] and ($\delta^{18}\mathrm{O} = 0.33 \cdot \mathrm{T} - 16.6$ ‰) Wassenaar et al. [50] reported similar correlations.

4.3. *$\delta^{2}H$ and $\delta^{18}O$ in surface waters*

The relationship of δ^{2}H and δ^{18}O values in surface waters in the inland PNW is presented in Figure 5 along with the inland PNW meteoric water line as reference. The surface water isotope data are presented in the Supplemental online materials (Table S6). As expected for a semi-arid region, surface water lines exhibit low slopes ranging from 3.99 to 6.09 and negative intercepts ranging from -18.02 ‰ to -50.1 ‰ indicating evaporation enrichment. In the Palouse Basin, the combination of low elevations, flat landscapes, and large surface travel times facilitate the evaporation enrichment along the stream networks as observed in Figure 5(a) and 5(b) (i.e. scattering below the LMWL). The isotopic composition of surface waters in mountainous watersheds is less variable, which is represented by a tight cluster of data points close to the mean annual isotopic composition of precipitation (Figure 5(c) and 5(d)).

Figure 6 shows the seasonal stream δ^{18}O variations compared to the volumetric discharge for all sampled streams. Stream δ^{18}O values in Crumarine Creek and the South Fork of the Palouse River (Pullman, WA) ranged from -13.7 ‰ to -17.7 ‰ (mean $= -15.2$ ‰) and from -12.9 ‰ to -17.7 ‰ (mean $= -15.0$ ‰) (Figure 6(a) and 6(b)), respectively. In the lower section of the Palouse Basin, δ^{18}O values in the South Fork and North Fork of the Palouse River (Colfax, WA) varied from -11.5 ‰ to -18.0 ‰ (mean $= -14.5$ ‰) and from -10.6 ‰ to -16.8 ‰ (mean $= -14.3$ ‰), respectively. By the outlet of the Palouse River (Hooper, WA), δ^{18}O values ranged from -12.5 ‰ to -17.8 ‰ (mean $= -14.1$ ‰) (Figure 6(c)). In the Silver Valley, stream δ^{18}O values in Canyon Creek and Pine Creek ranged from -14.2 ‰ to -17.0 ‰ (mean $= -15.8$ ‰) and from -14.5 ‰ to -16.2 ‰ (mean $= -15.3$ ‰) (Figure 6(d) and 6(e)), respectively. In the Priest River area, δ^{18}O values in Benton Creek and Priest River varied from -14.7 to -15.6 ‰ (mean $= -15.5$ ‰) and from -15.2 ‰ to -15.7 ‰ (mean $= -15.5$ ‰) (Figure 6(f) and 6(g)), respectively.

Despite the observed seasonal variation in precipitation in the inland PNW, seasonal stream δ^{18}O variations were very small. Standard deviations (1σ) of δ^{18}O values among all streams

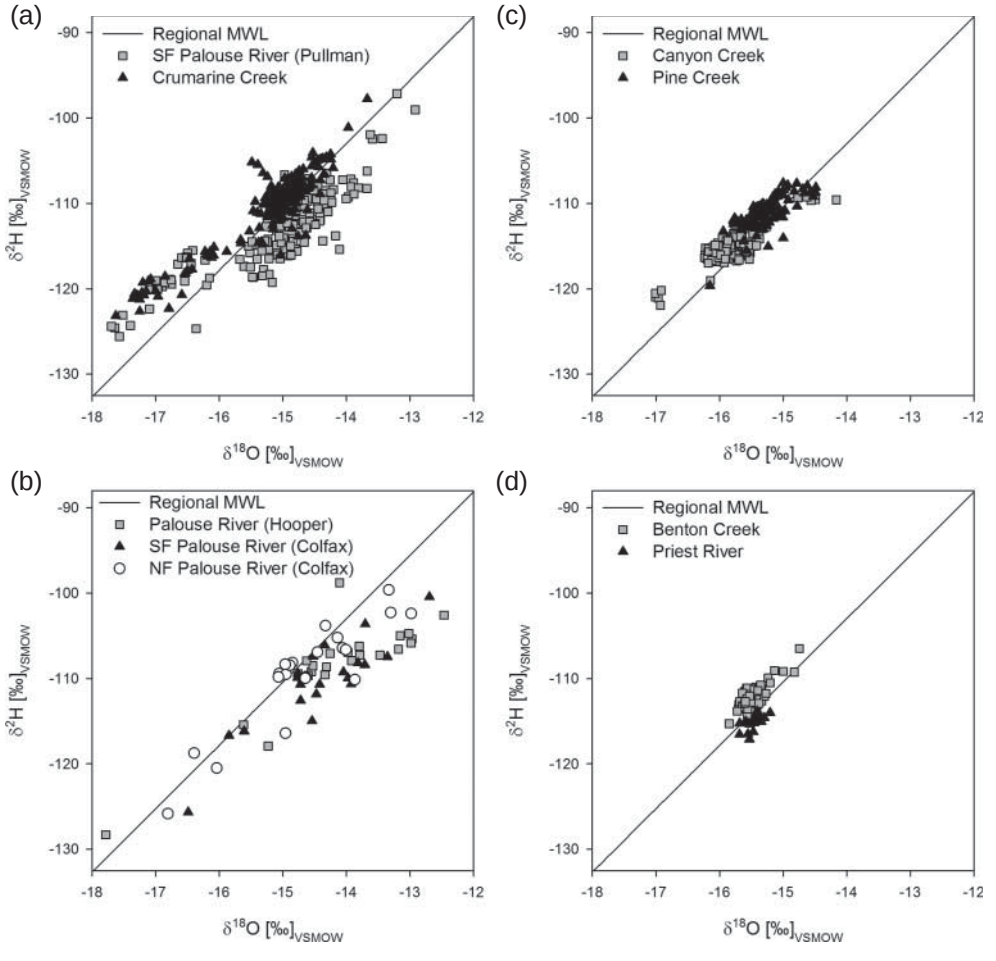

Figure 5. Isotopic composition of surface waters in the inland PNW, USA. The regional meteoric water line is plotted as reference ($\delta^2H = 7.42{\cdot}\delta^{18}O + 0.88$). (a) SF Palouse River (Pullman, WA): $\delta^2H = 4.52{\cdot}\delta^{18}O - 44.5$; $n = 195$, $r^2 = 0.73$. Crumarine Creek (Moscow, ID): $\delta^2H = 5.34{\cdot}\delta^{18}O - 29.3$; $n = 245$, $r^2 = 0.85$. (b) Palouse River (Hooper, WA): $\delta^2H = 4.47{\cdot}\delta^{18}O - 45.2$; $n = 24$, $r^2 = 0.76$. SF Palouse River (Colfax, WA): $\delta^2H = 5.02{\cdot}\delta^{18}O - 38.1$; $n = 23$, $r^2 = 0.88$. NF Palouse River (Colfax, WA): $\delta^2H = 4.88{\cdot}\delta^{18}O - 38.2$; $n = 23$, $r^2 = 0.86$. (c) Canyon Creek (Wallace, ID): $\delta^2H = 4.15{\cdot}\delta^{18}O - 49.4$; $n = 158$, $r^2 = 0.71$. Pine Creek (Pinehurst, ID): $\delta^2H = 3.99{\cdot}\delta^{18}O - 50.1$; $n = 143$, $r^2 = 0.48$. (d) Benton Creek (Priest River, ID): $\delta^2H = 6.09{\cdot}\delta^{18}O - 18.02$; $n = 84$, $r^2 = 0.66$. Priest River (Priest River, ID): $\delta^2H = 4.57{\cdot}\delta^{18}O - 44.5$; $n = 18$, $r^2 = 0.38$.

ranged from 0.13 ‰ (Priest River) to 1.44 ‰ (North Fork of the Palouse River) compared to the range of standard deviations in precipitation (3.52 ‰ Palouse region; 3.04 ‰ Silver Valley; 3.39 ‰ Priest River area). However, a large snowmelt event (26 March 2012) produced a considerable depletion in the isotopic composition of stream waters up to -18 ‰ $\delta^{18}O$ (Figure 6(a) and 6(b)). This snowmelt event was caused by a rapid warming up to 18 °C resulting in a large depleted runoff contribution. In the 2013 water year, snowmelt runoff was gradually resulting in less depleted runoff inputs to stream waters. Overall, $\delta^{18}O$ values during summer baseflow periods exhibited a closer composition to the mean annual $\delta^{18}O$ of precipitation whereas more depleted values were observed during winter and spring runoff events caused by depleted rains and snowmelt inputs. In the lower section of the Palouse Basin, a clear seasonal trend was observed with isotopic enrichment occurring in the summer time and depletion during the winter season (Figure 6(c)).

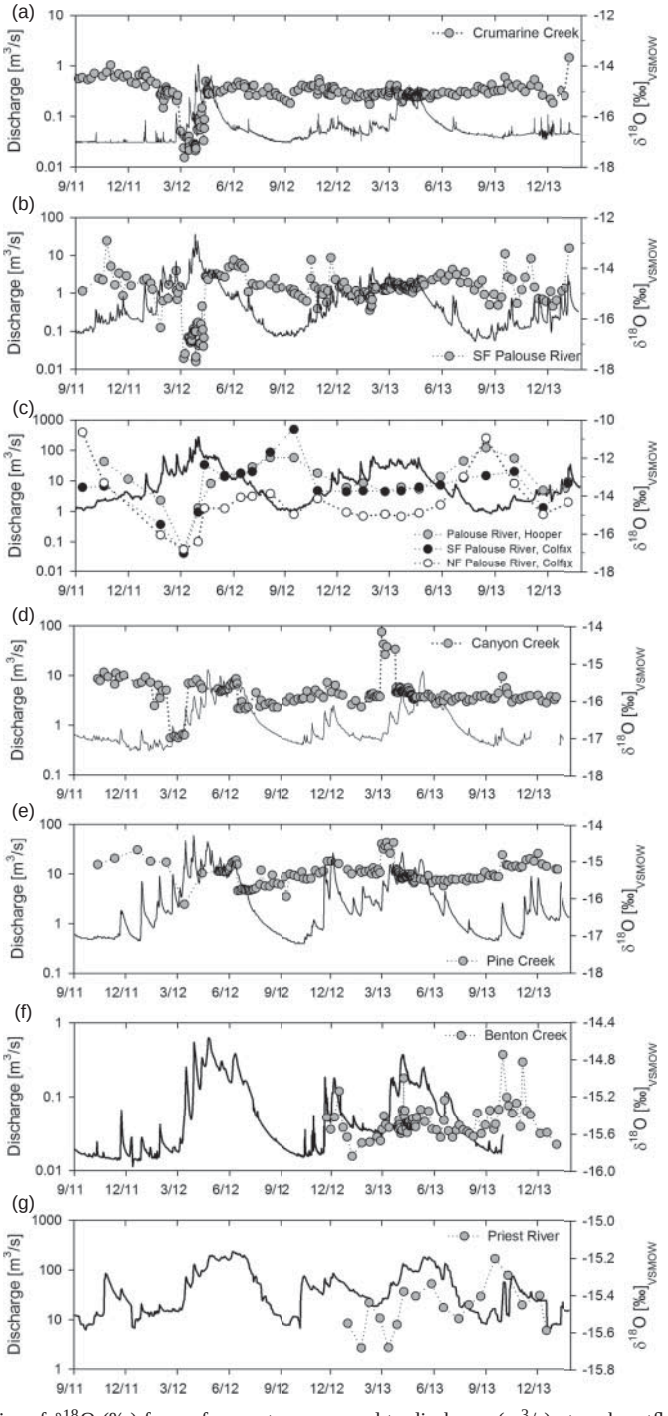

Figure 6. Time series of $\delta^{18}O$ (‰) for surface water compared to discharge (m^3/s) at each outflow location (a) Crumarine Creek, Moscow Mountain, Idaho [$A = 6.35\ km^2$]. (b) South Fork of the Palouse River, Pullman, Washington [$A = 342\ km^2$]. (c) Palouse River (grey circles) [$A = 6{,}472\ km^2$], Hooper, Washington; South Fork of the Palouse River (black circles) [$A = 709\ km^2$], Colfax, Washington; North Fork of the Palouse River (open circles) [$A = 1287\ km^2$], Colfax, Washington. Black line denotes the discharge of the Palouse River at Hooper, Washington. (d) Canyon Creek [$A = 60\ km^2$], Wallace, Idaho. (e) Pine creek [$A = 190\ km^2$], Pinehurst, Idaho. (f) Benton Creek [$A = 7.24\ km^2$], Priest River, Idaho. (g) Lower Priest River [$A = 2{,}335\ km^2$], Priest River, Idaho.

4.4. *$\delta^{18}O$ damping ratios and MTTs*

The relative age differences among the study watersheds can be shown by the damping ratio of the observed isotopic composition of precipitation in the observed stream water isotopic signal. Since the standard deviation of $\delta^{18}O$ in precipitation is quite similar across the inland PNW (3.04 ‰ to 3.39 ‰), the damping ratio highly depends on the stream $\delta^{18}O$ variability. Streams with a high groundwater contribution such as those found in forested watersheds tend to exhibit a fairly constant isotopic composition (Figure 6(d) – (f)), whereas human-altered watersheds where runoff is a dominant process tend to have a more variable $\delta^{18}O$ composition (Figure 6(b)). The damping ratios in the agricultural and urban-altered watersheds of Crumarine Creek and the South Fork of the Palouse River (Pullman, WA) were 0.20 and 0.25, respectively. In the Silver Valley area, the mining-altered watersheds of Canyon Creek and Pine Creek exhibited a damping ratio of 0.12 and 0.09, respectively. In contrast, in the Priest River area, the damping ratio of the pristine forested watershed of Benton Creek was 0.05.

Table 3 shows the baseflow mean transit times (bMTT) and goodness of fit metrics (i.e. EM, EPM, and DM models) for each selected watershed. In Crumarine Creek (6.35 km^2, 100 % granitic, human (urban and agricultural)-altered watershed), the best model fit ($r^2 = 0.41$; $\sigma = 0.056$ ‰) with the observed $\delta^{18}O$ values was exhibited by the EM which resulted in a bMTT of 1.0 year. Likewise, in Benton Creek (7.4 km^2, 65 % granitic, natural (forested)-watershed), the best TTD was described by EM ($r^2 = 0.25$; $\sigma = 0.045$ ‰) which translates in a bMTT of 3.2 years. The baseflow discharge behaviour within the human (mining)-altered watersheds dominated by sedimentary (63–66 %) and metamorphic (17 – 37 %) basement rocks was better described by the DM ($D_p = 0.6$). The bMTT were 1.5 and 0.7 years in Pine Creek ($r^2 = 0.34$; $\sigma = 0.042$ ‰) and Canyon Creek ($r^2 = 0.27$; $\sigma = 0.034$ ‰), respectively. The human (urban and agriculture)-altered watershed, South Fork of the Palouse River, as expressed in a high damping ratio ($D = 0.25$, Figure 7) was poorly correlated (Table 3) with all the weighting functions. Return flows such as irrigation or wastewater treatment plant outflow, especially during the summer season, could result in isotopic disturbances that may bias the $\delta^{18}O$ input–output relationship. In the South Fork of the Palouse River, bMTT ranged from 0.4 to 0.6 years. A high discrepancy was found between the evaluation of model simulations between the index of agreement d and the coefficient of determination r^2 (Table 4). Relative high d values (i.e. indicating strong data fits) usually over 0.65 have been reported as a disadvantage of this method [100]. In general, MAE (0.10 ‰ to 0.62 ‰) and RSME (0.13 ‰ to 0.74 ‰) indicated a low to moderate deviation from the $\delta^{18}O$ measurements.

A highly significant power regression ($\tau = 0.11D^{-1.09}$; $r^2 = 0.83$) was found between the bMTT and the damping ratio. A significant linear regression ($\tau = -10.9D + 2.93$; $r^2 = 0.65$, not shown in Figure 7) was also found. McGuire [82] reported a similar relationship ($\tau = -26.2D + 3.63$; $r^2 = 0.82$) in small catchments in the Western Cascades of Oregon.

Table 3. Baseflow bMTTs τ (years), goodness of fit σ (‰), and coefficient of determination r^2 for the EM, EMP, and DP models.

Site	EM			EPM ($\eta = 1.5$)			DM ($D_p = 0.6$)			DM ($D_p = 0.1$)		
	τ (yr)	σ (‰)	r^2	τ (yr)	σ (‰)	r^2	τ (yr)	σ (‰)	r^2	τ (yr)	σ (‰)	r^2
Crumarine Creek	**1.0**	**0.056**	**0.41**	0.7	0.084	0.03	0.9	0.056	0.19	0.9	0.063	0.11
SF Palouse River	0.6	0.138	0.01	**0.4**	**0.141**	**0.08**	0.5	0.124	0.05	0.6	0.161	0.01
Pine Creek	1.7	0.054	0.01	1.2	0.076	0.22	**1.5**	**0.042**	**0.34**	1.5	0.061	0.25
Canyon Creek	1.3	0.042	0.01	0.8	0.045	0.02	**0.7**	**0.034**	**0.27**	1.1	0.034	0.02
Benton Creek	**3.2**	**0.045**	**0.25**	0.7	0.057	0.16	2.8	0.055	0.16	2.9	0.096	0.01

Note: The best model results per study site are in bold.

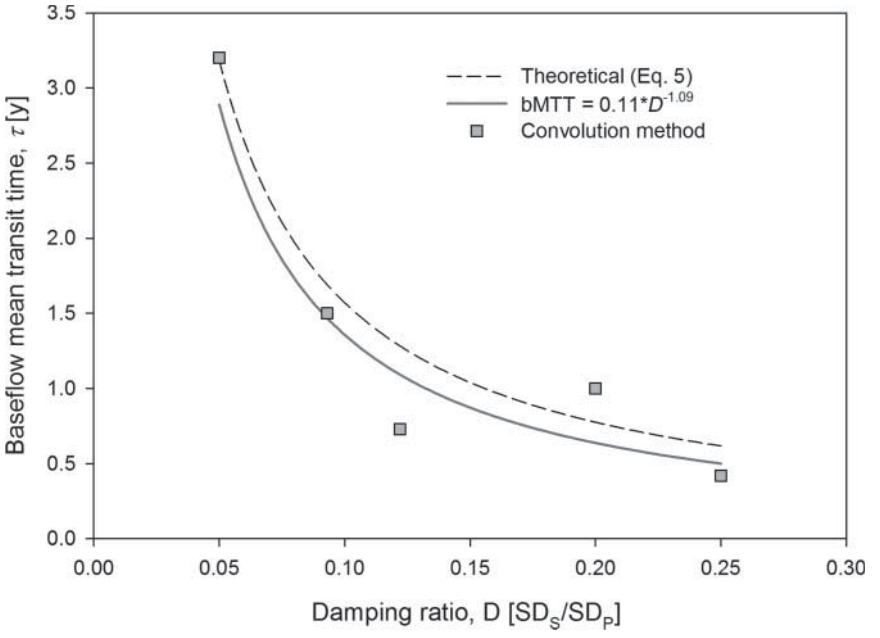

Figure 7. The relationship between baseflow MTT (τ) and the damping ratio of the standard deviations of $\delta^{18}O$ of stream water (SD_s) to precipitation (SD_p).

Overall, the relative MTT estimated by the sine-wave and periodic regression approach were slightly greater than the bMTT obtained with the lumped-parameter models. The relationship between the MTT and bMTT can be described as: bMTT = 1.03·MTT – 0.197; $r^2 = 0.93$. Although the sine-wave method is computationally simple, it does not allow for the evaluation of multiple TDD, since an exponential behaviour is assumed (see Equation 5). DeWalle et al. [81] and McGuire [82] have reported that the sine-wave can be used to estimate the potential maximum MTT that models are capable of simulating. Nevertheless, the use $\delta^{18}O$ input–output time series and damping ratios can be used to depict potential MTT bounds, which in turn are useful to evaluate contaminant degradation and transport times.

4.5. *Baseflow geochemistry*

Figure 8 shows the geochemical composition of major ions in surface waters of five selected watersheds (Crumarine Creek, South Fork of the Palouse River, Pine Creek, Canyon Creek, and Benton Creek) during the 2013 baseflow period. Additional geochemical information is presented in the Supplemental materials (Table S7). In line with the relative age estimates aforementioned, the human (urban and agriculture)-altered watersheds within the upper Palouse Basin presented a more dynamic geochemical composition over the recession period (Figure 8), whereas mountainous watersheds (Pine Creek, Canyon Creek, and Benton Creek) with greater MTTs presented a more homogenous geochemical composition.

The baseflow geochemistry of the South Fork of the Palouse River (Pullman, WA) was dominated by $Na - HCO_3$ type water (i.e. $Na > Ca > Mg > K$ and $HCO_3 > Cl > SO_4 > NO_3 > F > PO_4$) (Table S7) with electrical conductivities ranging from 411–731 µS/cm and slightly basic pH (7.4 – 8.1). Total alkalinity ranged from 120–170 mg/L $CaCO_3$. As shown in Figure 8, the geochemical composition of the South Fork of the Palouse River evolved towards greater Na and Cl concentrations over the baseflow recession, which may be an indication of irrigation

Table 4. Additional goodness of fit metrics for FLOWPC model simulations.

Site	EM			EPM ($\eta = 1.5$)			DM ($D_p = 0.6$)			DM ($D_p = 0.1$)		
	RMSE (‰)	MAE (‰)	*d*	RMSE (‰)	MAE (‰)	*d*	RMSE (‰)	MAE (‰)	*d*	RMSE (‰)	MAE (‰)	*d*
Crumarine Creek	0.26	0.21	0.85	0.39	0.36	0.69	0.35	0.30	0.86	0.32	0.29	0.80
SF Palouse River	0.63	0.52	0.45	0.65	0.53	0.29	0.57	0.47	0.41	0.74	0.62	0.33
Pine Creek	0.21	0.18	0.83	0.29	0.25	0.72	0.16	0.13	0.90	0.24	0.20	0.77
Canyon Creek	0.16	0.14	0.85	0.17	0.15	0.85	0.13	0.10	0.88	0.13	0.11	0.89
Benton Creek	0.17	0.13	0.87	0.21	0.16	0.76	0.21	0.16	0.78	0.36	0.33	0.71

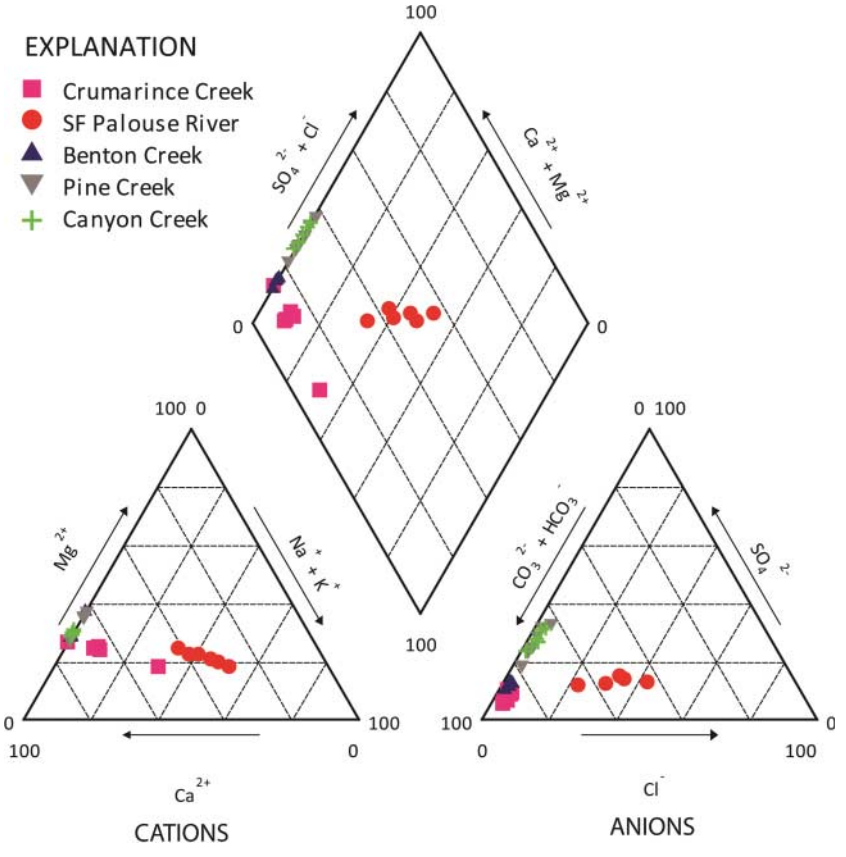

Figure 8. Piper diagram showing major ion composition in five watersheds in the inland PNW throughout the baseflow summer period in 2013.

return flows rather than reflecting a natural groundwater signal. In Crumarine Creek, the dominant type water was described by $Ca - HCO_3$ system ($Ca > Mg > K$ and $HCO_3 > SO_4 > Cl$), which comprised ~ 80 % of the total ion composition (Figure 8). Total alkalinity ranged from 20–26 mg/L $CaCO_3$. Electrical conductivity ranging from 32–50 μS/cm coupled with near neutral pH ($7.1 - 7.5$) may indicate relative short flow paths and infiltrated snowmelt contributions, which also presented a fairly constant isotopic composition compared to the South Fork of the Palouse River.

In the human (mining)-altered watersheds of the Silver Valley area, baseflow geochemical compositions were dominated by $Ca/Mg - HCO_3$ type water. Greater transit times (i.e. longer water–rock contact time) compared to those in the Palouse region are depicted by a more homogenous geochemical composition over the baseflow recession and a legacy of unique trace element fingerprints from the mining activity. In Canyon Creek and Pine Creek, total alkalinity ranged from $16 - 42$ mg/L $CaCO_3$ and $11 - 14$ mg/L $CaCO_3$, respectively. Canyon Creek presented greater electrical conductivities ($36 - 123$ µS/cm) than that of Pine Creek ($16 - 35$ µS/cm). Stream pH values were relatively similar with values ranging from $6.9 - 7.2$ and $7.3 - 7.7$ in Pine Creek and Canyon Creek, respectively. Sulphate constituted the second major anion with concentrations ranging from 4.8–15.5 mg/L in Canyon Creek and 2.1–5.4 mg/L in Pine Creek. Several heavy metals were detected in both streams (Ba, Cu, Mn, Zn, and Pb). Figure 9 shows the Zn and Pb total loads over the baseflow recession in Canyon Creek and Pine Creek. Zinc loads averaged 10 and 88 kg/d in Pine Creek and Canyon Creek, respectively. Zinc

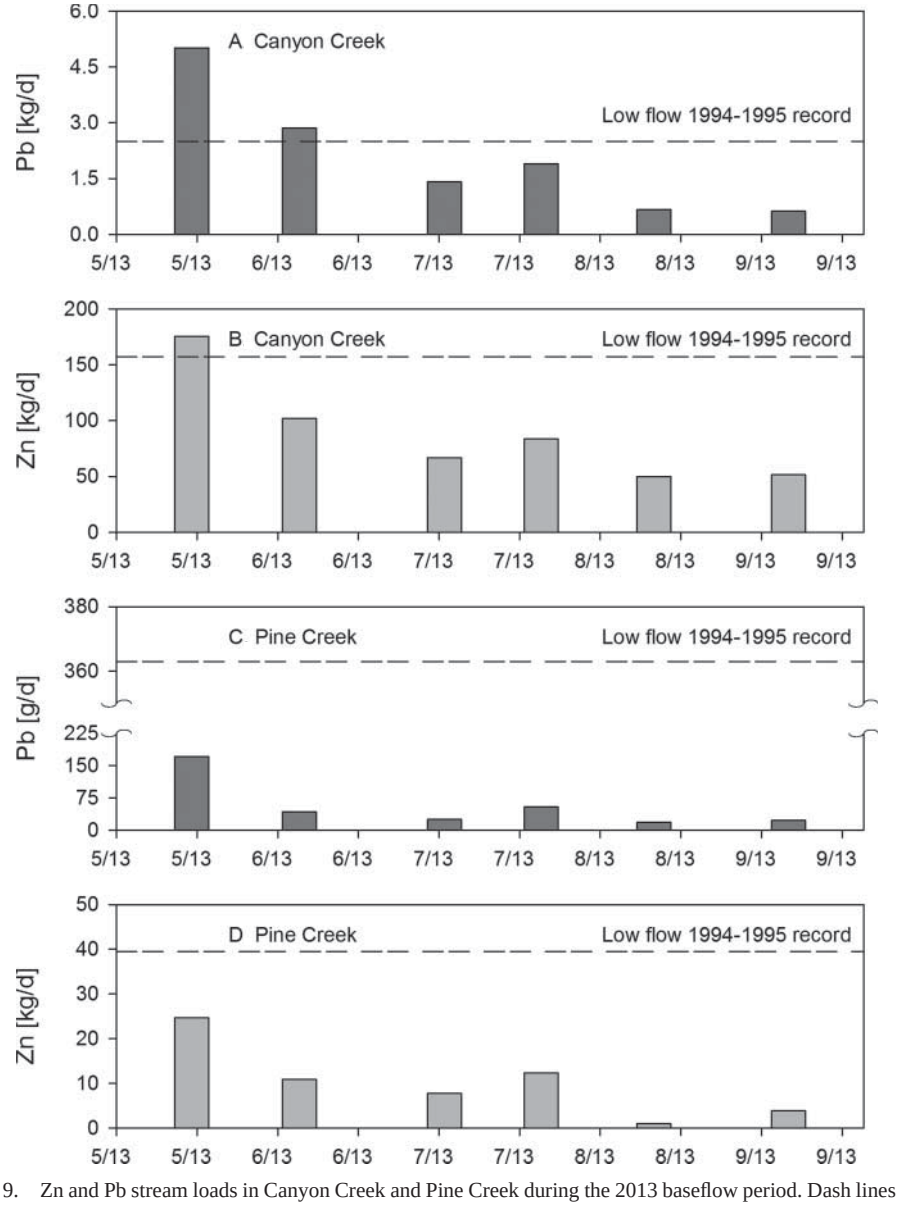

Figure 9. Zn and Pb stream loads in Canyon Creek and Pine Creek during the 2013 baseflow period. Dash lines denote historic Zn and Pb loads during the 1994–1995 baseflow recessions.

loads determined during the baseflow periods of 1994 and 1995 were 39.5 and 157 kg/d [79] in Pine Creek and Canyon Creek, respectively. Lead loads averaged 55 and 2.1 kg/d in Pine Creek and Canyon Creek, correspondingly. Lead loads determined during the baseflow periods of 1994 and 1995 were 363 and 2.5 kg/d [79] in Pine Creek and Canyon Creek, respectively. Even though significant reduction in the heavy metal transport has occurred in the study watersheds due to the absence of current explorations, the mining legacy is still an issue in the Silver Valley area, particularly during the summer months. The relatively large transit times (1.29–1.71 years) found in the area could facilitate the adsorption of heavy metals in the soil matrix, but also, due to massive mining alteration, could enhance the water–rock interaction bringing contaminant solute to the surface water system.

The geochemical composition of Benton Creek was mostly dominated by Ca/Mg – HCO_3 type water (Ca > Mg and HCO_3 > SO_4 > Cl). Electrical conductivity ranged from 35–50 µS/cm and slightly acid pH (6.7 – 7.3). Total alkalinity ranged from 18–24 mg/L $CaCO_3$. Nutrients (i.e. NO_3 and PO_4) and heavy metals were not detected. Overall, the geochemistry data in Benton Creek during the baseflow period indicated contribution of infiltrated snowmelt with relatively low-ion composition.

5. Conclusions

Isotope ratios in the inland PNW showed a temperature-dependent seasonality with a regional meteoric water line of $\delta^2H = 7.42 \cdot \delta^{18}O + 0.88$ ($n = 316$; $r^2 = 0.97$). Low d-excess values for precipitation in the inland PNW revealed the incorporation of local recycled water vapour into the travelling air masses and secondary basin scale evaporation processes. Despite the observed seasonal isotopic variation in precipitation, the seasonal stream $\delta^{18}O$ variation was very small. However, a significant depletion in surface waters was observed during the 2012 spring due to a large snowmelt event. Overall, the human-altered watershed on fractured basalt showed the greatest isotopic variability in streams, especially during the summer flows. Spatial isotopic differences in stream $\delta^{18}O$ time series across the study watersheds highlight the relative contributions of depleted groundwater reservoirs in the streamflow regime.

A highly significant power regression ($\tau = 0.11D^{-1.09}$; $r^2 = 0.83$) was found between the MTT and the damping ratio, indicating greater subsurface travel times as the observed damping ratio decreased. Natural watersheds exhibited a lower damping ratio whereas human-altered watersheds presented greater variability. Relative MTTs (i.e. sine-wave approach and damping ratio) and baseflow MTTs were greater in watersheds composed mainly of massive granitic formations and sedimentary basement rocks while watersheds in fractured basalt formations presented smaller travel times. Baseflow MTTs ranged from 0.4–0.6 years (human (urban and agriculture)-altered and fractured basalt-dominated landscape), 0.7–1.7 years (human (mining)-altered and predominantly sedimentary rocks), and 0.7 – 3.2 years (natural (forested) and granitic-dominated watersheds). Baseflow geochemical data provided complementary information regarding source water influences related to land use, such as irrigation return flows in agricultural watersheds, snowmelt, and infiltration in forested watersheds and mining legacies. Baseflow geochemical results supported the relative water age estimates. In mountainous watersheds with greater residence times, water chemistry was more homogenous whereas in the agricultural watersheds with smaller residence times, temporal variation in chemical composition was more dynamic.

Acknowledgements

The David Lamb Memorial Scholarship awarded by the Washington State Lake Protection Association (WALPA) to RSM covered a portion of the geochemical analyses.

Disclosure statement

No potential conflict of interest was reported by the authors.

Funding

This project was funded by the joint venture agreement [No. 10-JV-11221634–252] between USDA Forest Service Rocky Mountain Research Station and the University of Idaho.

Supplemental data

Supplemental data for this article can be accessed http://dx.doi.org/10.1080/10256016.2015.1008468.

References

[1] Lackey RT [internet]. Providing ecosystems services for an additional 50 + million PNW residents: the challenge to natural resource and environmental agencies [Internet]. Oregon State University, USA [cited 2014 March 22]. Available from: http://fw.oregonstate.edu/system/files/u2937/2013p%20-%20Pacific%20Northwest%202100%20Project%20-%20Web%20Description%20-%202013.pdf

[2] Callahan B, Miles E, Fluharty D. Policy implications of climate forecasts for water resources management in the Pacific Northwest. Policy Sci. 1999;32:269–293.

[3] Miles EL, Snover AK, Hamlet AF, Callahan B, Fluharty D. Pacific Northwest regional assessment: the impacts of climate variability and climate change on the water resources of the Columbia River Basin. JAWRA. 2000;36:399–420.

[4] Mote PW. Trends in snow water equivalent in the Pacific Northwest and their climatic causes. Geophys Res Lett. 2003;30:1601. Available from: http://ir.library.oregonstate.edu/xmlui/bitstream/handle/1957/18711/Mote_Geophys_Res_Lett_2003.pdf?sequence = 1

[5] Hamlet AF. Assessing water resources adaptive capacity to climate change impacts in the Pacific Northwest region of North America. Hydrol Earth Syst Sci. 2011;15:1427–1443.

[6] Chang H, Jung IW, Steele M, Gannett M. Spatial patterns of March and September streamflow trends in Pacific Northwest streams, 1958–2008. Geogr Anal. 2012;44:177–201.

[7] Wu H, Kimball JS, Elsner MM, Mantua N, Adler R, Stanford J. Projected climate change impacts on the hydrology and temperature of Pacific Northwest rivers. Water Resour Res. 2012;48:W11530.

[8] Sánchez-Murillo R, Brooks ES, Sampson L, Boll J, Wilhelm F. Ecohydrological analysis of steelhead (*Oncorhynchus mykiss*) habitat in an effluent dependent stream in the Pacific Northwest, USA. Ecohydrology. 2014;7:557–568.

[9] Rudestam K. Loving water, resenting regulation: sense of place and water management in the Willamette watershed. Soc Natur Resour. 2014;27:20–35.

[10] Berghuijs WR, Woods RA, Hrachowitz M. A precipitation shift from snow towards rain leads to a decrease in streamflow. Nat Clim Change. 2014;4:583–586.

[11] McCabe GJ, Clark MP. Trends and variability in snowmelt runoff in the Western United States. Hydrometeorology. 2005;6:476–482.

[12] van Kirk RW, Naman SW. Relative effects of climate and water use on base-flow trends in the lower Klamath basin. JAWRA. 2008;44:1032–1052.

[13] Elsner MM, Cuo L, Voisin N, Deems JS, Hamlet AF, Vano JA, Mickelson K, Lee S, Lettenmaier DP. Implications of 21st century climate change for the hydrology of Washington State. Clim Change. 2010;102:225–260.

[14] Mayer TD. Controls of summer stream temperature in the Pacific Northwest. Hydrology. 2012;475:323–335.

[15] Mote PW, Salathé EP. Future climate in the Pacific Northwest. Clim Change. 2010;102:29–50.

[16] Larson KR, Keller CK, Larson PB, Allen-King RM. Water resources implications of ^{18}O and ^{2}H distributions in a basalt aquifer system. Groundwater. 2000;38:947–953.

[17] Lyn B, Knobel L, Hall LF, DeWayne C, Green J. Development of a local meteoric water line for Southeastern Idaho, Western Wyoming, and South-central Montana. Idaho Falls (USA): U.S. Geological Survey Scientific Investigations Report 2004–5126. Prepared in cooperation with the U.S. Department of Energy; 2004.

[18] Goodwin AJ. Oxygen-18 in surface and soil waters in a dry land agricultural setting, eastern Washington: flow processes and mean residence times at various watersheds scales [thesis]. Pullman (WA): Washington State University; 2006.

[19] Koeniger P, Hubbart JA, Link T, Marshall JD. Isotopic variation of snow cover and streamflow in response to changes in canopy structure in a snow-dominated mountain catchment. Hydrol Process. 2008;22:557–566.

[20] Moravec BC, Keller KC, Smith JL, Allen-King RM, Goodwin AJ, Fairley JP, Larson PB. Oxygen-18 dynamics in precipitation and streamflow in a semi-arid agricultural watershed, Eastern Washington, USA. Hydrol Process. 2010;24:446–460.

[21] Moxley N. Stable isotope analysis of surface water and precipitation in the Palouse Basin: hydrologic tracers of aquifer recharge [Thesis]. Pullman (WA): Washington State University; 2012.

[22] Kendall C, McDonnell JJ, editors. Isotope tracers in catchment hydrology. Amsterdam: Elsevier; 1998.

[23] Berden G, Peeters R, Meijer G. Cavity ring-down spectroscopy: experimental schemes and applications. Int Rev Phys Chem. 2010;19:565–607.

[24] Lis GP, Wassenaar LI, Hendry MJ. High-precision laser spectroscopy D/H and $^{18}O/^{16}O$ measurements of microliter natural water samples. Anal Chem. 2008;80:287–293.

[25] Wen XF, Sun XM, Zhang SC, Yu GR, Sargent SD, Lee X. Continuous measurement of water vapor D/H and $^{18}O/^{16}O$ isotope ratios in the atmosphere. Hydrology. 2008;349:489–500.

[26] Gupta P, Noone D, Galewsky J, Sweeney C, Vaughn BH. Demonstration of high-precision continuous measurements of water vapor isotopologues in laboratory and remote field deployments using wavelength-scanned cavity ring-down spectroscopy (WS-CRDS) technology. Rapid Commun Mass Spectrom. 2009;23:2534–2542.

[27] Munksgaard NC, Wurster CM, Bass A, Bird MI. Extreme short-term stable isotope variability revealed by continuous rainwater analysis. Hydrol Process. 2012;26:3630–3634.
[28] Bernan ESF, Levin NE, Landais A, Li S, Owano T. Measurement of $\delta^{18}O$, $\delta^{17}O$, and ^{17}O-excess in water by off-axis integrated cavity output spectroscopy and isotope ratio mass spectrometry. Anal Chem. 2013;85:10392–10398.
[29] Koeniger P, Leibundgut C, Link T, Marshall J. Stable isotopes applied as water tracers in column and field studies. Org Geochem. 2010;41:31–40.
[30] Frederickson GC, Criss RE. Isotope hydrology and residence times of the unimpounded Meramec River Basin, Missouri. Chem Geol. 1999;157:303–317.
[31] McGuire KJ, DeWalle DR, Gburek DJ. Evaluation of mean residence in subsurface waters using oxygen-18 fluctuations during drought conditions in the mid-Appalachians. Hydrology. 2002;261:132–149.
[32] Rodgers P, Soulsby C, Waldron S, Tezlaff D. Using stables isotopes tracers to assess hydrological flow paths, residence times and landscape influence in a nested mesoscale catchment. Hydrol Earth Syst Sci. 2005;9: 139–155.
[33] Uchida T, McDonell JJ, Asano Y. Functional intercomparison of hillslopes and small catchments by examining water source, flowpath and mean residence time. Hydrology. 2006;327:627–642.
[34] Tezlaff D, Soulsby C, Hrachowitz M, Speed M. Relative influence of upland and lowland headwaters on the isotope hydrology and transit time of larger catchments. Hydrology. 2011;400:438–447.
[35] Asano Y, Uchida T. Flow path depth is the main controller of mean base flow transit times in a mountainous catchment. Water Resour Res. 2012;48:W03512.
[36] Dansgaard W. Stable isotopes in precipitation. Tellus. 1964;16:436–468.
[37] Merlivat L, Jouzel J. Global climatic interpretation of the deuterium–oxygen 18 relationship for precipitation. Geophys Res. 1979;84:4918–4922.
[38] Rozanski K, Araguás-Araguás LJ, Gonfiantini R. Relation between long-term trends of oxygen-18 isotope composition of precipitation and climate. Science. 1992;258:981–985.
[39] Araguás-Araguás L, Froehlich K, Rozanski K. Deuterium and oxygen-18 isotope composition of precipitation and atmospheric moisture. Hydrol Process. 2000;14:1341–1355.
[40] Bowen G, Revenaugh J. Interpolating the isotopic composition of modern meteoric precipitation. Water Resour Res. 2003;39:1299. Available from: http://onlinelibrary.wiley.com/doi/10.1029/2003WR002086/abstract
[41] Aggarwal PK, Alduchov OA, Froehlich KO, Araguas-Araguas LJ, Sturchio NC, Kurita N. Stable isotopes in global precipitation: a unified interpretation based on atmospheric moisture residence time. Geophys Res Lett. 2012;39:L11705.
[42] Sánchez-Murillo R, Esquivel-Hernández G, Welsh K, Brooks ES, Boll J, Alfaro-Solís R, Valdés-González J. Spatial and temporal variation of stable isotopes in precipitation across Costa Rica: an analysis of historic GNIP records. Open J Mod Hydrol. 2013;3:226–240.
[43] Craig H. Isotopic variations in meteoric waters. Science. 1961;133:1702–1703.
[44] Jouzel J, Hoffmann G, Koster RD, Masson V. Water isotopes in precipitation: data/model comparison for present day and past climates. Quat Sci Rev. 2000;19:363–379.
[45] Cappa CD, Hendricks MB, DePaolo DJ, Cohen RC. Isotopic fractionation of water during evaporation. Geophys Res. 2003;108:4525–4534.
[46] Birkel C, Soulsby C, Tezlaff D, Dunn S, Spezia L. High-frequency storm event isotope sampling reveals time-variant transit time distributions and influence of diurnal cycles. Hydrol Process. 2012;26:308–316.
[47] McGlynn B, McDonnel JJ, Brammer DD. A review of the evolving perceptual model of hillslope flowpaths at the Maimai catchments, New Zealand. Hydrology. 2002;257:1–26.
[48] Tezlaff D, Soulsby C. Towards simple approaches for mean residence time estimation in ungauged basins using tracers and soil distributions. Hydrology. 2008;363:60–74.
[49] Speed M, Tezlaff D, Soulsby C, Hrachowitz M, Waldron S. Isotopic and geochemical tracers reveal similarities in transit times in contrasting mesoscale catchments. Hydrol Process. 2010;24:1211–1224.
[50] Wassenaar LI, Athanasopoulos P, Hendry MJ. Isotope hydrology of precipitation, surface and ground waters in the Okanagan Valley, British Columbia, Canada. Hydrology. 2011;411:37–48.
[51] Rozanski K, Araguas-Araguas LJ, Gonfiantini R. Isotopic patterns in modern global precipitation. In: Swart PK, Lohmann KC, McKenzie J Savin S, editors. Climate change in continental isotopic records. No 67, Geophysical Monograph; Washington (USA): American Geophysics Union; 1993.
[52] Froehlich K, Gibson JJ, Aggarwal P. Deuterium excess in precipitation and its climatological significance. Study of environmental change using isotope techniques. C&S Papers Series 13/P. Vienna (Austria): International Atomic Energy Agency; 2002.
[53] Dunn SM, McDonnell JJ, Vaché KB. Factors influencing the residence time of catchment waters: a virtual experiment approach. Water Resour Res. 2007;43:W06408.
[54] Soulsby C, Tetzlaff D, Hrachowitz M. Tracers and transit times: windows for viewing catchment scale storage? Hydrol Process. 2009;23:3503–3507.
[55] Stewart MK, Morgenstern U, McDonnell JJ, Pfister L. The 'hidden streamflow' challenge in catchment hydrology: a call to action for stream water transit time analysis. Hydrol Process. 2012;26:2061–2066.
[56] Kim S, Jung S. Estimation of mean water transit time on a steep hillslope in South Korea using soil moisture measurements and deuterium excess. Hydrol Process. 2014;28:1844–1857.
[57] Godsey SE, Aas W, Clair TA, de Wit HA, Fernandez IJ, Kahl SJ, Malcolm IA, Neal C, Neal M, Nelson SJ, Norton SA, Palucis MC, Skjelkvåle BL, Soulsby C, Tetzlaff D, Kirchner JW. Generality of fractal 1/f scaling in

catchment tracer time series, and its implications for catchment travel time distributions. Hydrol Process. 2010;24: 1660–1671.
[58] Hrachowitz H, Soulsby C, Tetzlaff D, Malcolm A, Schoups G. Gamma distribution models for transit time estimation in catchments: physical interpretation of parameters and implications for time-variant transit time assessment. Water Resour Res. 2010;46:W10536.
[59] van der Velde Torfs PJJF, van der Zee SEATM, Uijlenhoet R. Quantifying catchment-scale mixing and its effect on time-varying travel time distributions. Water Resour Res. 2012;48:W06536.
[60] Hrachowitz M, Savenije H, Bogaard TA, Tetzlaff D, Soulsby C. What can flux tracking teach us about water age distribution patterns and their temporal dynamics? Hydrol Earth Syst Sci. 2013;17:533–564.
[61] Asano Y, Uchida T, Ohte N. Residence times and flow paths of water in steep unchannelled catchments, Tanakami, Japan. Hydrology. 2002;261:173–192.
[62] Broxton PD, Troch PA, Lyon SW. On the role of aspect to quantify water transit times in small mountainous catchments. Water Resour Res. 2009;45:W08427.
[63] Soulsby C, Tetzlaff D, Rodgers P, Dunn SM, Waldron S. Runoff processes, stream water residence times and controlling landscape characteristics in a mesoscale catchment: an initial evaluation. Hydrology. 2006;325:197–221.
[64] McGuire KJ, McDonnell JJ, Weiler M, Kendall C, McGlynn BL, Welker JM, Seibert J. The role of topography on catchment-scale water residence time. Water Resour Res. 2005;41:W05002.
[65] Viville D, Ladouche B, Bariac T. Isotope hydrological study of mean transit time in the granitic Strengbach catchment (Vosges massif, France): application of the FlowPC model with modified input function. Hydrol Process. 2006;20:1737–1751.
[66] Katsuyama M, Tani M, Nishimoto S. Connection between streamwater mean residence time and bedrock groundwater recharge/discharge dynamics in weathered granite catchments. Hydrol Process. 2010;24:2287–2299.
[67] Capell R, Tetzlaff D, Hartley AJ, Soulsby C. Linking metrics of hydrological function and transit times to landscape controls in a heterogeneous mesoscale catchment. Hydrol Process. 2012;26:405–420.
[68] Heidbüchel I, Troch PA, Lyon SW. Separating physical and meteorological controls of variable transit times in zero-order catchments. Water Resour Res. 2013;49:7644–7657.
[69] Maloszewski P, Zuber A. Determining the turnover time of groundwater systems with the aid of environmental tracers, I. Models and their applicability. Hydrology. 1982;57:207–231.
[70] Maloszewski P, Zuber A. Lumped parameter models for the interpretation of environmental tracer data. Manual on mathematical models in isotope hydrology. IAEA-TECDOC 910. Vienna (Austria): IAEA; 1996.
[71] McGuire KJ, McDonell JJ. A review and evaluation of catchment transit time modeling. Hydrology. 2006;330:543–563.
[72] Zuber A. Mathematical models for the interpretation of environmental radioisotopes in groundwater systems. In: Fontes PFJC, editor. Handbook of environmental isotope geochemistry, Vol. 2. Amsterdam: Elsevier; 1986. p. 9–58.
[73] Hall M, Young DL, Walker DJ. Agriculture in the Palouse: a portrait of diversity. Moscow, Idaho: University of Idaho, Agricultural Communications, Bulletin 794; 1999.
[74] Brooks ES, Boll J, McDaniel PA. Hydropedology in seasonally dry landscapes: the Palouse region of the Pacific Northwest USA. In: Lin, H, editor. Hydropedology: synergistic integration of soil science and hydrology. Amsterdam: Academic Press, Elsevier B.V.; 2012. p. 329–350.
[75] Murray J, O'Green AT, McDaniel PA. Development of a GIS database for ground-water recharge assessment of the Palouse Basin. Soil Sci. 2003;168:759–768.
[76] Palouse Basin Aquifer Committee (PBAC). Palouse ground water basin water use report. Pullman-Moscow Area (USA); 2012 [cited 2014 April 1]. Available from: http://www.webpages.uidaho.edu/pbac/
[77] Mitchell V, Reed L, Larsen J. Geology of northern Idaho and the Silver Valley. Idaho Geological Survey. Idaho State University [cited 2014 January 15]. Available from: http://geology.isu.edu/Digital_Geology_Idaho/Module7/mod7.htm
[78] Horowitz AJ, Elrick KA, Cook RB. Effect of mining and related activities on the sediment trace element geochemistry of Lake Coeur D'Alene, Idaho, USA. Part I: Surface sediments. Hydrol Process. 1993;7: 403–423.
[79] Silver Valley Natural Resources Trustees. Canyon Creek response actions 1995–1999. Idaho: Kellog; 2000.
[80] Dougthy PT, Price RA. Tectonic evolution of the Priest River complex, northern Idaho and Washington – a reappraisal of the Newport fault with new insights on metamorphic core complex formation. Tectonics. 1999;18:375–393.
[81] DeWalle DR, Edwards PJ, Swistock BR, Aravena R, Drimie RJ. Seasonal isotope hydrology of three Appalachian forest catchments. Hydrol Process. 1997;11:1895–1906.
[82] McGuire KJ. Water residence time and runoff generation in the western Cascades of Oregon [dissertation]. Corvallis, Oregon: Oregon State University; 2004.
[83] Maloszewski P. Lumped-parameter models as a tool for determining the hydrological parameters of some groundwater systems based on isotope data. Tracers and Modeling in Hydrogeology. Proceedings of the TraM'2000 Conference held at Liège; 2000 May; Belgium. IAHS; 2000.
[84] Zuber A, Weise SM, Motyka J, Osenbrück K, Różański K. Age and flow pattern of groundwater in a Jurassic limestone aquifer and related Tertiary sands derived from combined isotope, noble gas and chemical data. Hydrology. 2004;286:87–112.

[85] Katz BG, Chelette AR, Pratt TR. Use of chemical and isotopic tracers to assess nitrate contamination and groundwater age, Woodville Karst Plain, USA. Hydrology. 2004;289:36–61.
[86] Einsiedl F, Maloszewski F, Stichler W. Multiple isotope approach to the determination of the natural attenuation potential of a high-alpine karst system. Hydrology. 2009;365:113–121.
[87] Stumpp C, Maloszewski P, Stichler W, Fank J. Environmental isotope (δ^{18}O) and hydrological data to assess water flow in unsaturated soils planted with different crops: case study lysimeter station "Wagna" (Austria). Hydrology. 2009;369:198–208.
[88] Willmot CJ. On the validation of models. Phys Geogr. 1981;2:184–194.
[89] Legates DR, McCabe GJ Jr. Evaluating the use of "goodness-of-fit" measures in hydrologic and hydroclimatic model validation. Water Resour Res. 1999;35:233–241.
[90] USEPA. Methods for the Chemical Analysis of Water and Wastes (MCAWW) (EPA/600/4-79/020) EPA Method 310.1: alkalinity; 1978. Available from: https://www.nemi.gov/methods/method_summary/5230/
[91] USEPA. Determination of inorganic ions by ion chromatography. EPA Method 300. Revision 2.1; 1993. Available from: http://water.epa.gov/scitech/methods/cwa/bioindicators/upload/2007_07_10_methods_method_300_0.pdf
[92] USEPA. Trace elements in water, solids, and biosolids by inductively coupled plasma-atomic emission spectroscopy. EPA Method 200.7. Revision 4.4; 2001. Available from: http://water.epa.gov/scitech/methods/cwa/bioindicators/upload/2007_07_10_methods_method_200_7.pdf
[93] USEPA. Trace elements in water, solids, and biosolids by inductively coupled plasma-mass spectroscopy. EPA Method 200.8. Revision 5.4; 2007. Available from: http://water.epa.gov/scitech/methods/cwa/bioindicators/upload/2007_07_10_methods_method_200_8.pdf
[94] GNIP. Global Network of Isotopes in Precipitation. International Atomic Energy Agency [cited 2014 January 15]; 2006. Available from: http://www naweb.iaea.org/napc/ih/IHS_resources_gnip.html
[95] Peng H, Mayer B, Harris S, Krouse HR. A 10-yr record of stable isotope ratios of hydrogen and oxygen in precipitation at Calgary, Alberta, Canada. Tellus. 2004;56B:147–159.
[96] Miyake Y, Matsubaya O, Nishihara C. An isotopic study on meteoric precipitation. Pap Meteorol Geophys. 1968;19:243–266.
[97] Steward MK. Stable isotope fractionation due to evaporation and isotopic exchange of falling water drops: applications to the atmospheric processes and evaporation of lakes. Geophys Res. 1975;80:1133–1146.
[98] Jouzel J. Isotopes in cloud physics: multiphase and multistage condensation processes. In: Fritz BP, Fontes JC, editors. Handbook of environmental isotope geochemistry, Vol. 2: the terrestrial environment. Amsterdam: Elsevier; 1986. p. 117–152.
[99] Jouzel J, Merlivat L. Deuterium and oxygen-18 in precipitation: modelling of the isotopic effect during snow formation. Geophys Res. 1984;89:11749–11757.
[100] Krause P, Boyle DP, Bäse F. Comparison of different efficiency criteria for hydrological model assessment. Adv Geosci. 2005;5:89–97.